Journal of Materials Science: Materials in Medicine (2025)36:98
https://doi.org/10.1007/s10856-025-06952-w

DELIVERY SYSTEMS

Original Research

Contribution of molecular-modified biomimetic mesoporous silica xerogel in delivering nimesulide with superior anti-inflammatory efficacy

Liu Yang[1] · Nan Yan[2] · Jing Li[1]

Received: 8 June 2025 / Accepted: 24 September 2025

Abstract

High efficiency of anti-inflammatories for anti-inflammatory drugs has enormous room for improvement, aiming to reduce side effects. Herein, molecular-modified biomimetic mesoporous silica xerogel was applied to establish a superior carrier for delivering nimesulide (NMS). Small molecules of chiral threonine and chiral malic acid, as well as a polymer of hydroxypropyl methylcellulose K250 (HPMC), were used to respectively obtain LT-MSX, DT-MSX, LM-MSX, DM-MSX, BMSX, L-BMSX, M-BMSX, and H-BMSX. Morphology and porous structure of the obtained carriers were analyzed, and properties of NMS-loaded carriers were studied by focusing on drug crystal form and molecule interactions. In vitro carrier degradation and drug release, as well as in vivo anti-inflammatory effects of drug-loaded carriers, were evaluated. The results demonstrated that the addition of molecules significantly impacted the porous properties of carriers. In addition, all these carriers improved drug release by converting the drug crystal form to an amorphous state. The swelling inhibition rate of NMS-loaded LT-MSX and NMS-loaded DT-MSX was the best, owing to their fast drug release and silica degradation, which can be of great value for the application of anti-inflammatory drugs.

Graphical Abstract

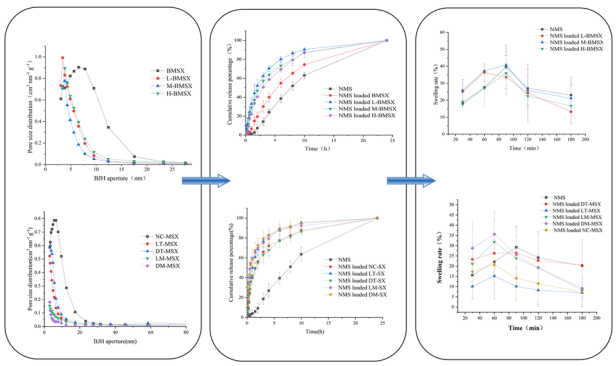

1 Introduction

Among all available drug biomaterials, mesoporous silica has been studied in many research works due to its unique properties. (1) Large surface area and pore volume provide great potential for adsorption and loading of drug molecules into pore channels; (2) The excellent mesoporous structure and adjustable pore size enable better control of drug

These authors contributed equally: Liu Yang, Nan Yan

✉ Jing Li
dddefghijklmn@163.com

[1] School of Pharmacy, Shenyang Medical College, Shenyang, Liaoning Province, China

[2] Department of Medical Applied Technology, Shenyang Medical College, Shenyang, Liaoning Province, China

Published online: 03 November 2025

loading and release kinetics; (3) Easily modified surfaces for controlled and targeted drug delivery enhance therapeutic efficacy and reduce toxicity; (4) In vivo biosafety evaluations of cytotoxicity, biodegradation, biodistribution and excretion have yielded satisfactory results; (5) Combinations with magnetic and/or luminescent compounds allow simultaneous applications of drug delivery and bioimaging; (6) Superior surface properties and porosity have been proven to be attractive candidates as bioactive materials for bone regeneration [1–5]. Based on these advantages, the studies on mesoporous silica materials have increased dramatically, especially in the field of intelligent drug delivery systems. It has been reported that mesoporous silica nanoparticles, as a safe oral drug carrier, have no toxicity to the simulated intestinal cells Caco-2 [6]. Current animal experiments have shown that mesoporous silica nanoparticles have two main in vivo excretion pathways: one is excreted by urine through renal filtration, the other is excreted by the liver into bile and feces, and urine excretion is the main excretion pathway of mesoporous silica nanoparticles [7].

Biomimetics usually refers to the technology that mimics or uses the structure, biochemical function, and biochemical process of the organism [8–10]. The cell wall of diatoms and the bone needle of sponges have exquisite nano-silica structures, and the formation of these structures can be guided by amino-rich molecules (amino acids, polyamines, peptides, polysaccharides, etc.). The use of biomimetic methods to construct mesoporous silica has attracted much attention in recent years. The biomimetic synthesis technology requires mild conditions. First, a self-assembly of organic matter is formed, and the inorganic precursor chemically reacts at the phase interface between the self-assembled aggregate and the solution. Under the action of the self-assembly template, an inorganic-organic complex is established [11–15]. Since mesoporous silica can flexibly modify molecules to regulate drug delivery, it is of great interest to study the effects of small molecules and polymers on the properties of biomimetic mesoporous silica.

Inflammation is defined as a vascular defense response of living tissues to resist the cumulative damage caused by inflammatory factors. Consequently, inflammation can lead to the occurrence and aggravation of many diseases, such as osteoarthritis (OA) and inflammatory bowel disease, etc. OA is the most common type of arthritis, which can affect major joints throughout the body, including the knee and elbow joints. In severe cases, it can even result in disability and is often referred to as "undying cancer." Acute gouty arthritis is a frequently encountered condition in emergency and outpatient settings. Its clinical symptoms include redness, swelling, heat, and pain in the affected joint. The incidence of this disease is increasing, and the age of patients is becoming younger. Clinical studies have found that this disease can directly impair joint function [16–22]. Nimesulide (NMS), a non-steroidal anti-inflammatory drug [4], is a selective cyclooxygenase-2 inhibitor, which is primarily used to treat chronic arthritis and other inflammatory conditions. After oral administration, it exerts analgesic, antipyretic, and anti-inflammatory effects. However, NMS has poor absorption and low bioavailability due to its low solubility, which significantly limits its clinical application. Therefore, enhancing the anti-inflammatory efficacy of NMS is highly necessary [23–26].

In this study, polyethylene imine (PEI) was employed as a biomimetic template, with chiral threonine and hydroxypropyl methylcellulose (HPMC) introduced as modulating groups to construct an NMS drug delivery system based on a biomimetic mesoporous silica framework. Threonine is a white rhomb or crystalline powder with odorless and taste slightly sweet, and it is mainly used in medicine, chemical reagents, food fortifiers, feed additives, and other aspects. Malic acid, also known as 2-hydroxybutanedioic acid, has two stereoisomers due to an asymmetric carbon atom in its structure. In nature, it exists in three forms: D-malic acid, L-malic acid, and their mixture, DL-malic acid. Malic acid is mainly used in the food and pharmaceutical industries. HPMC is a cellulose ether widely used in drug formulations due to its biocompatibility, uncharged nature, solubility in water, and thermoplastic behavior, and HPMC K250 belongs to one type of HPMC. By investigating the changes in drug properties before and after drug loading, in vitro drug release, and anti-inflammatory efficacy, the critical role of molecular groups in the delivery of drugs via biomimetic mesoporous silica carriers was elucidated. It was found that a series of mesoporous silica xerogel carriers showed similar characteristics in structure, all of which were composed of silica particles with internal pore structure, and had good drug loading performance. During drug loading, drug molecules could be converted into amorphous states, effectively improving the solubility and release of drugs, and the anti-inflammatory effect of drug-loaded carriers was better than that of the raw drug. The present study has important implications for the development of novel anti-inflammatory drug delivery systems.

2 Materials and methods

2.1 Materials

L-malic acid (≥99%), D-malic acid (≥99%), L-threonine (≥99%), D-threonine (≥99%), tetramethyl orthosilicate (TMOS) (≥99%), PEI (≥99%) were purchased from Dalian Meilun Biological Co., Ltd (China). Other chemical reagents are purchased from Tianjin Damao Chemical Reagent Factory (Tianjin, China). Deionized water was

prepared by the ion exchange method. All animal experiments in this study were conducted according to the Guidelines for the Care and Use of Laboratory Animals, that was authorized by the Ethics Review Committee for Animal Experimentation of Shenyang Medical College (Shenyang, Liaoning, China).

2.2 Synthesis of drug carriers

An appropriate amount of polyethylene imine (PEI_S) was weighed and dissolved in distilled water to obtain a PEIs aggregate solution with a concentration of 0.5 wt%. A certain dosage of HPMC K250 was used and dissolved in distilled water to prepare solutions with concentrations of 0.001 g/mL, 0.025 g/mL, and 0.05 g/mL, respectively.

Two milliliters of the PEIs aggregate solution was placed in a 10 mL vial, and 5 mL of the absolute ethanol mixture of TMOS was added, and then 1 mL of each of the three different concentrations of HPMC solution was added in the corresponding group. At room temperature, it was sealed, left to stand, dried, ground into fine powder, and sieved through a 100-mesh sieve to obtain BMSX, L-BMSX, M-BMSX, and H-BMSX.

Specific masses of LT-MSX, DT-MSX, LM-MSX, and DM-MSX were separately dissolved in distilled water to prepare 0.1 g/mL solutions of chiral threonine and chiral malic acid. 2 mL of the PEI aggregate solution was added to 2.5 mL of tetramethoxysilane (TMOS) anhydrous ethanol mixture. The above solution was homogeneously mixed at 25 °C to form a wet gel and finally dried to get a xerogel. Next, TMOs anhydrous ethanol mixture, PEI aggregate solution, and solutions of L-threonine, L-malic acid, D-threonine, and D-malic acid were respectively added. The mixture was shaken at 25 °C to yield the wet gel. Finally, the wet gel was dried, ground, and sieved to obtain NC-MSX, LT-MSX, DT-MSX, LM-MSX, and DM-MSX.

2.3 Properties of drug carriers

2.3.1 Scanning electron microscope(SEM)

The morphology of the carrier was characterized by SEM (JSM-7610FPlus, Japan); the sample was pasted onto a metal stigma and sputtered with gold under vacuum conditions.

2.3.2 Fourier-transform infrared (FT-IR)

Potassium bromide (KBr) pellets were fixed on a sample holder. Clear spectral graphs were obtained by using an FT-IR spectrometer (WQF-530, China). Then BMSX, L-BMSX, M-BMSX, H-BMSX, NC-MSX, LT-MSX, DT-MSX, LM-MSX, and DM-MSX were measured respectively in the spectral region of 400–4000 cm^{-1} to obtain the characteristics and absorption peaks of the samples.

2.3.3 Analysis of specific surface area and pore size

Nitrogen adsorption/desorption of BMSX, L-BMSX, M-BMSX, H-BMSX, NC-MSX, LT-MSX, DT-MSX, LM-MSX, and DM-MSX were measured using a specific surface area analyzer (Autosorb-iQ-MP, USA) to study their specific surface area and pore structure. All samples were degassed by vacuum drying at 150 °C to remove the adsorbed moisture.

2.3.4 Degradation of drug carriers

The degradation of the carrier is mainly determined by the silicon molybdenum blue colorimetric method. 5 g ammonium molybdoate was dissolved in 100 mL deionized water to prepare a 0.05 g/mL ammonium molybdoate solution. One gram citric acid and 5 g of ascorbic acid were mixed into 100 mL of deionized water to prepare the mixed acid solution. The carrier was degraded in vitro using the paddle method (100 rpm, 37 °C). 2 mg, 4 mg, 6 mg, 8 mg, 10 mg, 15 mg, 20 mg, and 30 mg of BMSX, L-BMSX, M-BMSX, and H-BMSX were respectively put into small cups, and then 200 mL of the dissolution medium with pH 6.8 phosphate buffer solution (PBS) was added to each small cup. At 15 min, 30 min, 45 min, 1 h, and 2 h, 5 mL of dissolved samples were taken out for measurement, and then 5 mL of ammonium molybdate solution and 5 mL of mixed acid solution were added to these samples at the same time. After 1 min, the color change of the solution was observed, followed by the quick measurement of absorbance at 838 nm. Similarly, the carriers of NC-MSX, LT-MSX, DT-MSX, LM-MSX, and DM-MSX were degraded by the paddle method (100 rpm, 37 °C). 2 mg, 4 mg, 6 mg, 8 mg, 10 mg, 15 mg, 20 mg, 30 mg NMS, NC-MSX, LT-MSX, DT-MSX, LM-MSX, DM-MSX were put into a small cup, and 200 mL of dissolved medium (pH 6.8) was added. Five milliliters of the dissolved sample were taken out at 15 min, 30 min, 45 min, 1 h, and 2 h, respectively. Subsequently, 5 mL of ammonium silicate solution and 5 mL of mixed acid solution were added to these samples at the same time point. Color changes were observed after 1 min, and absorbance was rapidly measured using a UV spectrophotometer (UV-1801, China) at 838 nm.

2.4 Preparation of the drug-loaded carrier

0.05 g/mL NMS was prepared using chloroform. 0.15 g BMSX, L-BMSX, M-BMSX, and H-BMSX were, respectively, added into 1 mL NMS solution, which was placed on a magnetic stirrer and stirred for 12 h (avoid light). The

obtained drug solution was first dried in a vacuum drying oven at 40 °C. After washing and centrifuging the drug solution twice, it was dried in an electric heating drying oven at 60 °C to obtain NMS loaded BMSX, NMS loaded L-BMSX, NMS loaded M-BMSX, and NMS loaded H-BMSX.

0.5 g of NMS was dissolved using chloroform to get a 0.05 g/mL NMS solution. NC-MSX, LT-MSX, DT-MSX, LM-MSX, and DM-MSX (0.3 g) were added to 2 mL of NMS chloroform solution and stirred with a magnetic stirrer for 12 h (avoid light). After vacuum drying for 4 h, the materials were washed with water, centrifuged, and dried at 60 °C to obtain NMS loaded NC-MSX, NMS loaded LT-MSX, NMS loaded DT-MSX, NMS loaded LM-MSX, and NMS loaded DM-MSX.

2.5 Properties of drug-loaded carrier

2.5.1 Determination of drug loading amount

Five milligrams each of NMS loaded BMSX, NMS loaded L-BMSX, NMS loaded M-BMSX, NMS loaded H-BMSX, NMS loaded NC-MSX, NMS loaded LT-MSX, NMS loaded DT-MSX, NMS loaded LM-MSX, and NMS loaded DM-MSX were precisely weighed and placed in a 10 mL volumetric flask using absolute ethanol, then sonicated in an ultrasonic washer for 20 min. The obtained solution was filtered through a 0.45 μm organic filter membrane, and the absorbance was used to calculate the drug loading capacity.

$$\text{Drug loading capacity}(\%) = \left(W_{\text{drugcontained in carrier}}/W_{\text{carrier}}\right) \times 100$$

2.5.2 Differential scanning calorimeter (DSC)

Under the protection of nitrogen, the heat flow maps of NMS, NMS loaded BMSX, NMS loaded L-BMSX, NMS loaded M-BMSX, and NMS loaded H-BMSX were measured by DSC (HSC-4, China) with the samples placed in an aluminum disk and heated from 70 °C to 300 °C at a heating rate of 5 °C/min.

The heat flow diagrams of NMS, NC-MSX, LT-MSX, DT-MSX, LM-MSX, DM-MSX, NMS loaded NC-MSX, NMS loaded LT-MSX, NMS loaded DT-MSX, NMS loaded LM-MSX, and NMS loaded DM-MSX were measured by DSC (HSC-4, China). The samples were placed in aluminum pans and heated from 25 °C to 300 °C at a heating rate of 5 °C/min under nitrogen protection.

2.5.3 FT-IR

The spectra of NMS, NMS loaded BMSX, NMS loaded L-BMSX, NMS loaded M-BMSX and NMS loaded H-BMSX were obtained in the spectral region of 400–4000 cm^{-1}. The potassium bromide was prepared, fixed on the sample rack, and the clear spectral map was obtained by a Fourier infrared spectrometer (WQF-530, China). Then, NMS loaded NC-MSX, NMS loaded LT-MSX, NMS loaded DT-MSX, NMS loaded LM-MSX, and NMS loaded DM-MSX were respectively measured to obtain the characteristics and absorption peaks of the samples.

2.5.4 In vitro drug release

The in vitro drug release was carried out by the stirring method (RC806D, China). Firstly, 5 mg of NMS, NMS loaded BMSX, NMS loaded L-BMSX, NMS loaded M-BMSX, and NMS loaded H-BMSX containing 5 mg of NMS were precisely weighed and then put into 300 mL pH 6.8 PBS, respectively. Then, the mixtures were stirred at 100 rpm. After each sampling, 5 mL pH 6.8 PBS (same temperature and same volume) was supplemented. Next, the sample was filtered, the absorbance was measured, the cumulative release percentage was calculated, and the dissolution curve was finally drawn.

The release of NMS loaded NC-MSX, NMS loaded LT-MSX, NMS loaded DT-MSX, NMS loaded LM-MSX, and NMS loaded DM-MSX were also studied using the stirring method. 300 mL of pH 6.8 PBS was added to small cups, and the experiment was carried out in an isothermal dissolution apparatus at 37 °C and 100 rpm. Five milligrams of NMS and NMS loaded NC-MSX, NMS loaded LT-MSX, NMS loaded DT-MSX, NMS loaded LM-MSX, and NMS loaded DM-MSX containing 5 mg of NMS were separately poured into small cups containing 300 mL pH 6.8 PBS. At the designed time points, a 5 mL sample was removed from the small cup, and the 5 mL sample was filtered by a 0.45 μm water system microporous filter membrane. The absorbance was measured by UV with pH 6.8 PBS as the reference. The cumulative release percentage was calculated, and the dissolution curve was plotted.

2.6 Anti-inflammatory experiment in rats

A number of male SD rats weighing 200 ± 20 g were randomly divided into five groups:

Group 1: normal saline group
Group 2: NMS group
Group 3: NMS loaded L-BMSX group
Group 4: NMS loaded M-BMSX group
Group 5: NMS loaded H-BMSX group

1% carrageenan saline solution was selected as the inflammatory inducer. Before administration, the rats were fasted for 12 h while being allowed free access to water.

Firstly, 1% carrageenan saline solution was obtained, and four normal saline suspensions containing the same amount of NMS and four normal saline suspensions containing the same amount of IMC were prepared. Next, the first group with the same amount of normal saline and the other groups with the prepared drug saline suspensions were orally administered. Thirty minutes later, 1% carrageenan saline solution was subcutaneously injected into the right hind toe of each rat. Subsequently, the ankle circumference of the right hind foot was measured at intervals of 30, 60, 90, 120, and 180 min to calculate the swelling degree, swelling rate, and swelling inhibition rate.

$$\text{Swelling degree} = \text{circumference after treatment} - \text{circunference before treatment}$$

$$\text{Swelling rate}(\%) = \text{Swelling degree}/\text{circumference before treatment} \times 100$$

$$\text{Swelling inhibition rate}(\%) = (\text{circumference of model group} - \text{circunference of drug group})/\text{circumference of model group} \times 100$$

1% carrageenan saline solution was used as an inducer in a rat model of inflammation. Fourteen male SD rats weighing 200 ± 20 g were randomly divided into seven groups:

Group 1. NMS raw material group
Group 2. NMS L-malic acid carrier group
Group 3. NMS D-malic acid carrier group
Group 4. NMS L-threonine carrier group
Group 5. NMS D-threonine carrier group
Group 6. NMS blank carrier group
Group 7. Saline control group

Rats were fasted for 12 h before administration and had free access to water. Five different drug-loaded normal saline suspensions (NMS, 32 mg/kg) were prepared. The rats in the normal saline group were given 2 mL of normal saline by gavage, and the rats in the other groups were orally given 2 mL of the drug, and the circumference of the right hind ankle was measured at determined time points. 1% carrageenan solution was subcutaneously injected into the right hind toe of each rat, and the ankle circumference of the right hind foot was measured at predetermined time intervals, including 30, 60, 90, 120, and 180 min.

3 Results and discussion

3.1 Properties of the carrier

3.1.1 SEM

According to the SEM result in Fig. 1, BMSX, L-BMSX, M-BMSX, and H-BMSX were accumulated by silica particles because PEIs, as a biomimetic template, increased the speed of the deposition of silicon source, and therefore the particles were in a stacked state to construct pores. As seen in Fig. 2, the silica stacking of NC-MSX was stronger than that of several chiral carriers, and the silica stacking of LT-MSX was stronger than that of DT-MSX, which can make more gaps for drug loading. After grinding, the particle size of NC-MSX was relatively uniform, while the particle size of the hand-type carrier was relatively uneven due to grinding.

3.1.2 FT-IR

Figure 3 shows that PEIs and HPMC were successfully used in the carrier. In addition, L-BMSX presented Si–O–Si bending vibration peak, Si–O–Si symmetric stretching vibration peak, and Si–O–Si asymmetric stretching vibration peak at 460.90 cm^{-1}, 794.52 cm^{-1}, and 950.73 cm^{-1}, respectively, indicating that L-BMSX was successfully synthesized.

Since the synthesis of several carriers was similar, LT-MSX was used as an example. There was a carbonyl stretching vibration peak at 1641.1 cm^{-1} for LT-MSX. Additionally, there was a bending vibration peak of Si–O–Si at 484.4 cm^{-1}, a symmetric stretching vibration peak of Si–O–Si at 790.7 cm^{-1}, an asymmetric stretching vibration peak of Si–O–Si at 1415.2 cm^{-1}, and a hydrogen bond vibration peak formed by Si–OH and N–H at 3369.2 cm^{-1}. From these characteristics, it can be inferred that LT-MSX was a synthesized silica material.

3.1.3 Specific surface area and pore size

According to Fig. 4A, C, it was clear that all drug carriers presented a hysteresis loop, confirming their mesoporous structure [27–30]. The addition of small molecules or polymers can significantly reduce specific surface area and pore volume evidenced by the reduction of specific surface area and pore volume shown in Table 1. Furthermore, the specific surface area and pore volume of LM-MSX and DM-MSX were obviously lower than those of LT-MSX and DT-MSX, demonstrating that different small molecules can

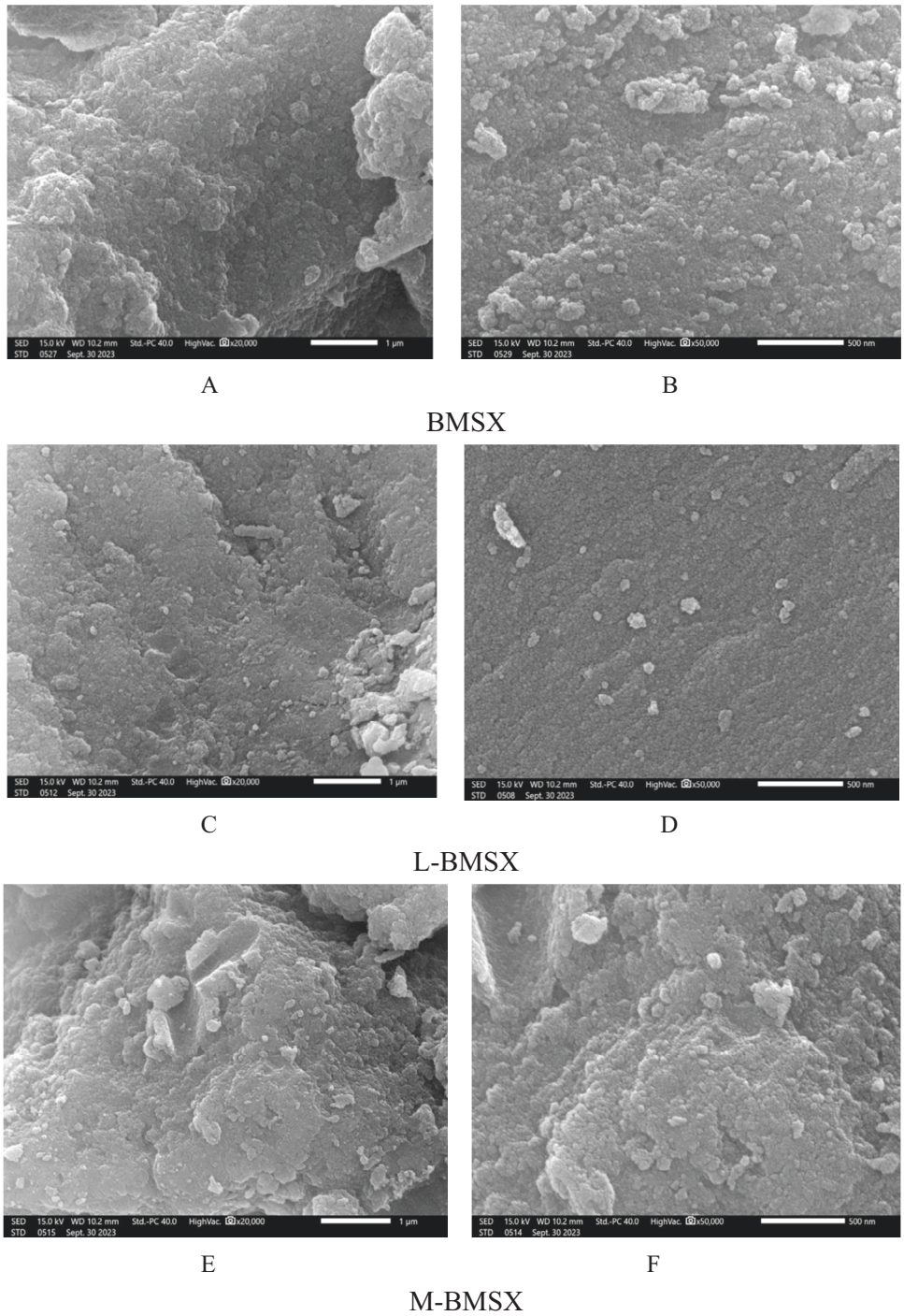

Fig. 1 SEM images of **A** and **B**, BMSX; **C** and **D**, L-BMSX; E and F, M-BMSX

have varied effects on specific surface area and pore volume. The main chemical structure difference between threonine and malic acid can be concluded as threonine contains an amino group, while malic acid consists of an extra carboxyl group, and an amino group catalyzes the hydrolysis and silica condensation during the formation of silica frame, resulting in a larger specific surface area and pore volume of LT-MSX and DT-MSX. However, the mean pore diameter of carriers was not regularly impacted by adding small molecules or polymer in the system. The pore size of carriers can be obviously affected by introducing small molecules or polymer, both for BMSX and NC-MSX (BMSX: 6.669 nm, L-BMSX: 3.502 nm; M-BMSX: 3.837 nm; H-BMSX: 3.878 nm; NC-MSX: 6.220 nm; LT-MSX: 3.119 nm; LM-MSX: 3.010 nm; DT-MSX: 3.557 nm; DM-MSX: 3.010 nm), indicating that the

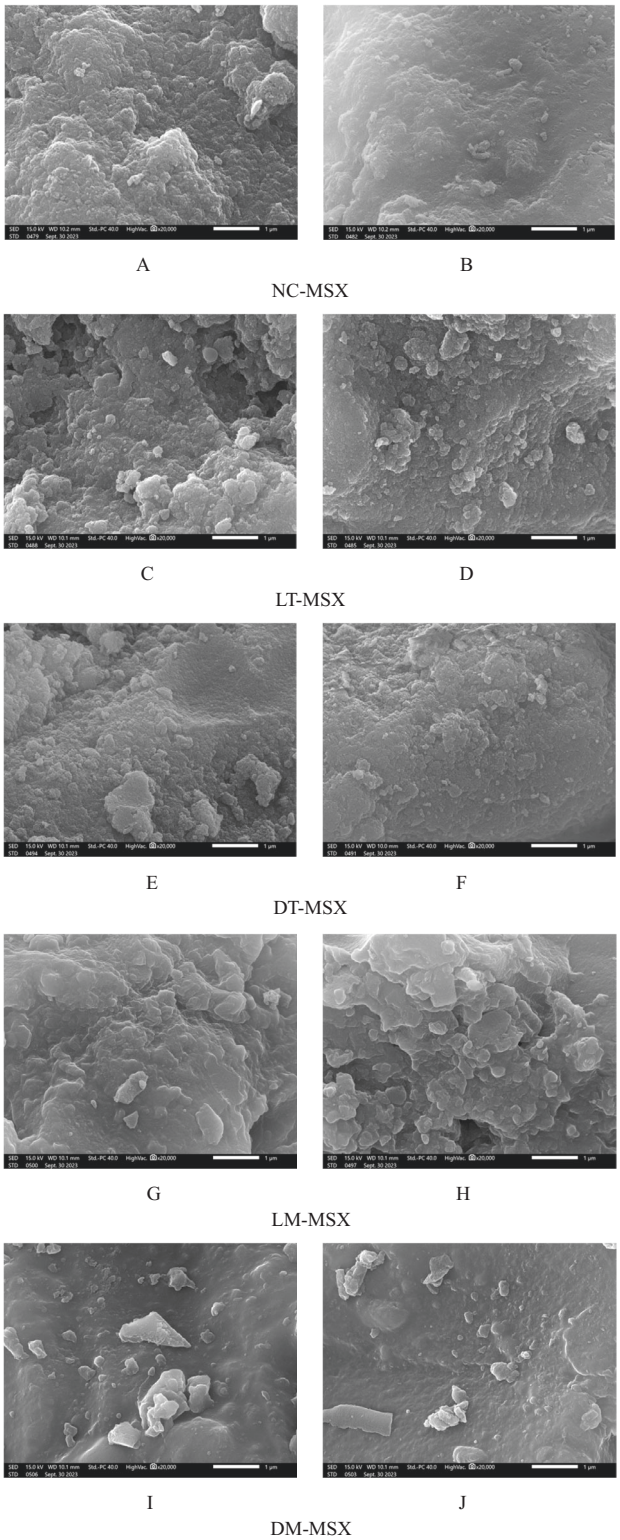

Fig. 2 SEM images of **A** and **B**, NC-MSX; **C** and **D**, LT-MSX; **E** and **F**, DT-MSX; **G** and **H**, LM-MSX; **I** and **J**, DM-MSX

introduction of small molecules or polymer in MSX mainly lowered pore size because these molecules were stored in the pores.

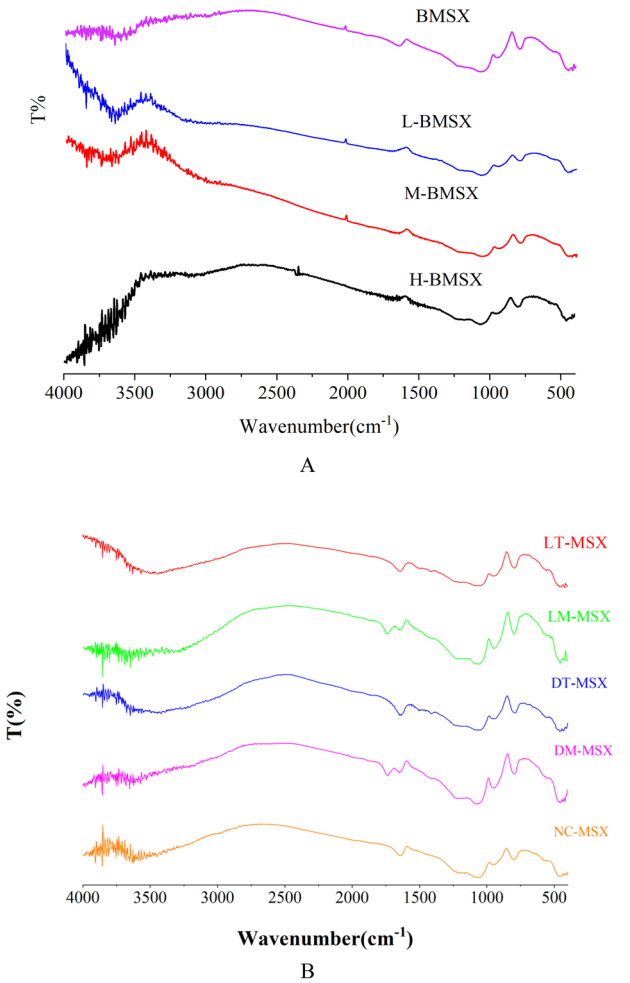

Fig. 3 IR spectra of **A**, BMSX, L-BMSX, M-BMSX, and H-BMSX; **B**, NC-MSX, LT-MSX, DT-MSX, LM-MSX, and DM-MSX

3.1.4 Degradation

With the time passed, the darker blue of the solution led to greater measured absorbance, indicating that the three carriers were gradually degraded. Figure 5 shows that the initial degradation of NMS loaded BMSX was higher than that of NMS loaded L-BMSX, NMS loaded M-BMSX, and NMS loaded H-BMSX, showing that HPMC can delay silica degradation owing to reduced specific surface area and pore volume. Among these carriers, the silica degradation at 120 min of NMS loaded L-BMSX was the least, which may relate to the property that most pore size of L-BMSX was the smallest Fig. 6. On the contrary, the addition of threonine in MSX significantly accelerated silica degradation, possibly (see Fig. 7) because the amino group on MSX for LT-MSX and DT-MSX enhanced silica degradation rate. The absorbance value of NMS loaded LM-MSX was lower than that of NMS loaded NC-MSX, so NMS loaded LM-MSX had an inhibitory effect compared with NMS loaded NC-MSX. The

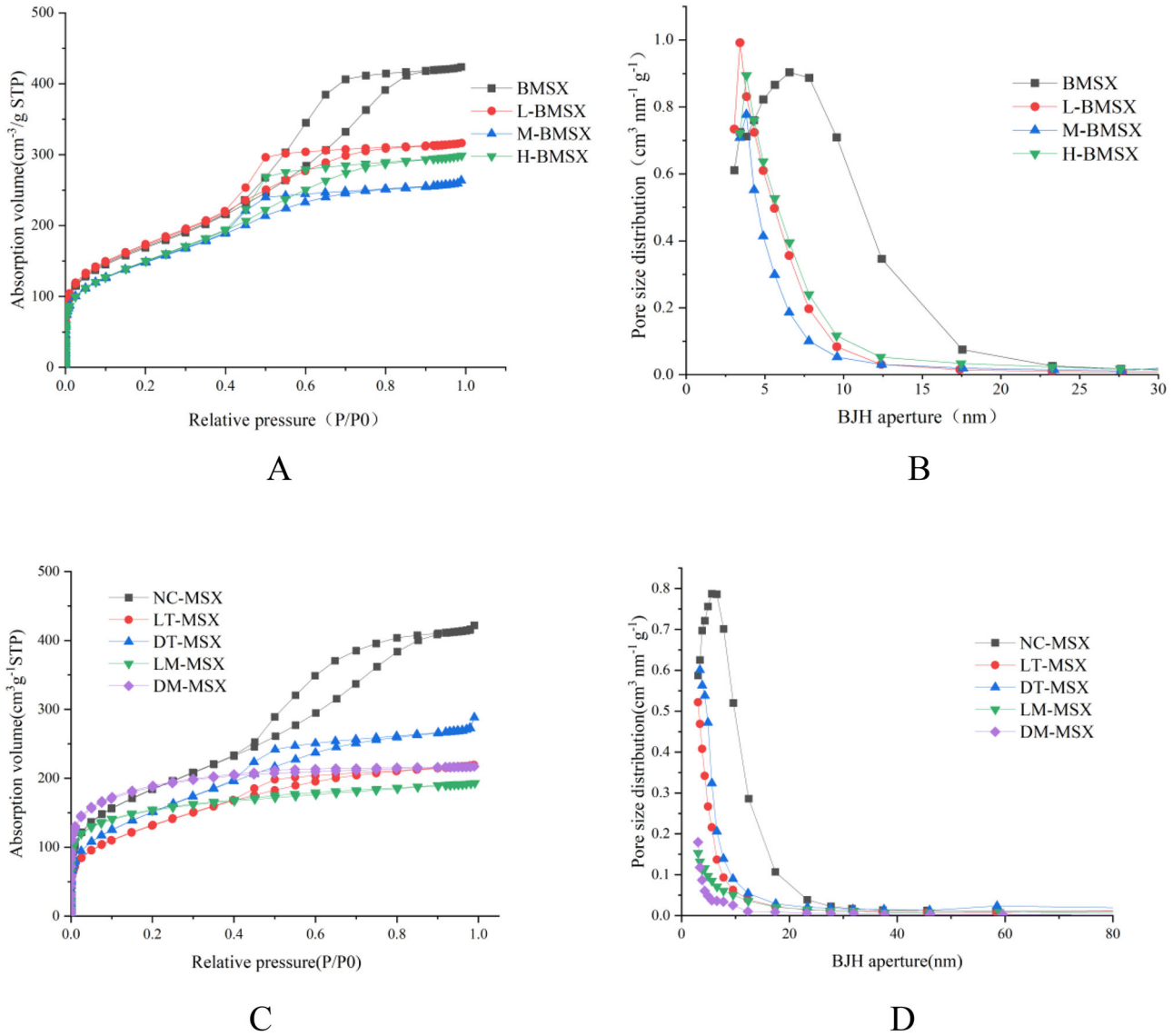

Fig. 4 **A** Nitrogen adsorption/desorption curves of BMSX, L-BMSX, M-BMSX, and H-BMSX; **B** pore distribution curves of BMSX, L-BMSX, M-BMSX, and H-BMSX; **C** nitrogen adsorption/desorption curves of NC-MSX, LT-MSX, DT-MSX, LM-MSX, and DM-MSX; **D** pore distribution curves of NC-MSX, LT-MSX, DT-MSX, LM-MSX, and DM-MSX

Table 1 Porous structure results of carriers

Sample	Specific surface area (m^2/g)	Pore volume (cm^3/g)	Pore diameter (nm)
BMSX	449.546	0.544	3.813
L-BMSX	341.428	0.325	3.502
M-BMSX	245.392	0.243	3.409
H-BMSX	336.692	0.334	3.831
LT-MSX	163.583	0.167	3.406
DT-MSX	201.181	0.238	3.398
LM-MSX	41.555	0.058	3.825
DM-MSX	40.150	0.041	3.055
NC-MSX	427.875	0.511	3.829

reason was that the steric hindrance induced by levorotatory carboxyl group modification, which prevented direct contact between the silica and the dissolution medium, while the dextral carboxyl group can have faster silica degradation for MSX. Since LM-MSX and DM-MSX had quite low specific surface area and pore volume, the modified groups presented important effects on silica degradation.

3.2 Properties of drug-loaded carriers

3.2.1 Drug loading

According to the results of drug loading in Table 2, all these carriers exhibited relatively high drug loading

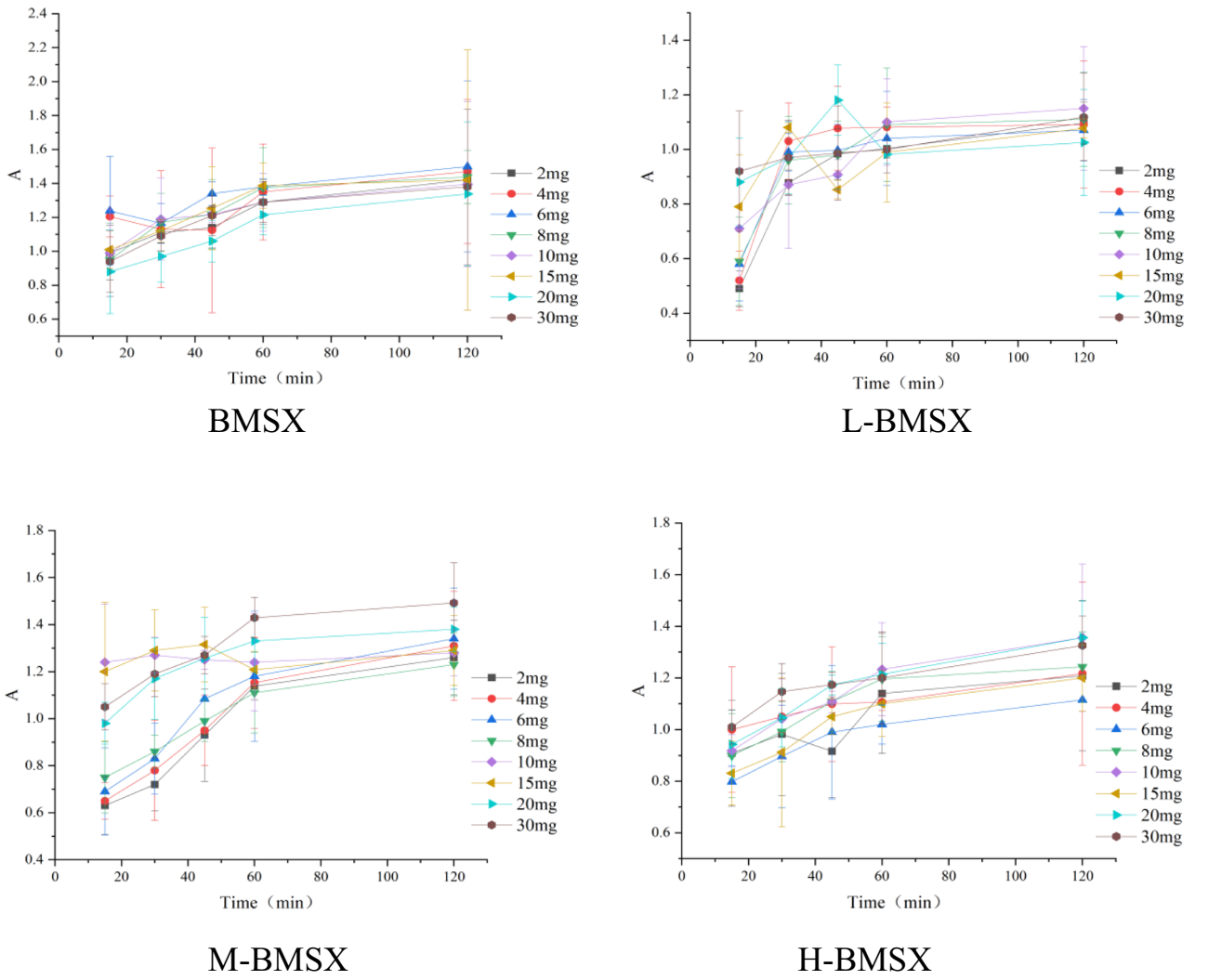

Fig. 5 Silica degradation of BMSX, L-BMSX, M-BMSX, and H-BMSX

capacities. NMS loaded L-BMSX had the lowest drug loading capacity, which can be ascribed to its smallest pore size. Moreover, the order of drug loading capacity was NMS loaded L-BMSX < NMS loaded M-BMSX < NMS loaded BMSX < NMS loaded H-BMSX, demonstrating that the addition of HPMC with a high amount can improve drug loading, possibly because the proper pore size of 3.878 nm can be favorable for loading NMS. In addition, it also reflected that the drug loading capacity result (NMS loaded L-BMSX < NMS loaded M-BMSX < NMS loaded H-BMSX) was directly related to the pore size of carriers (L-BMSX: 3.502 nm; M-BMSX: 3.837 nm; H-BMSX: 3.878 nm). As for another group of drug loading results, it was obvious that LT-MSX and DT-MSX loaded more NMS than LM-MSX and DM-MSX owing to the fact that LT-MSX and DT-MSX had higher specific surface area, pore volume, and pore size. Therefore, it revealed that the porous structure of MSX was crucial for obtaining the desired NMS loading capacity, among which pore size was the most important parameter. Furthermore, the introduction of threonine or a proper amount of HPMC can contribute to achieving high NMS loading.

3.2.2 DSC

As seen in Fig. 8, the results of DSC showed that the melting point peak of NMS was at about 152 °C, showing its crystal form. After loading into MSX carriers, only a quite small peak can be observed, demonstrating that most NMS was in an amorphous form in carriers [31–35]. It should be noted that the small peak of NMS

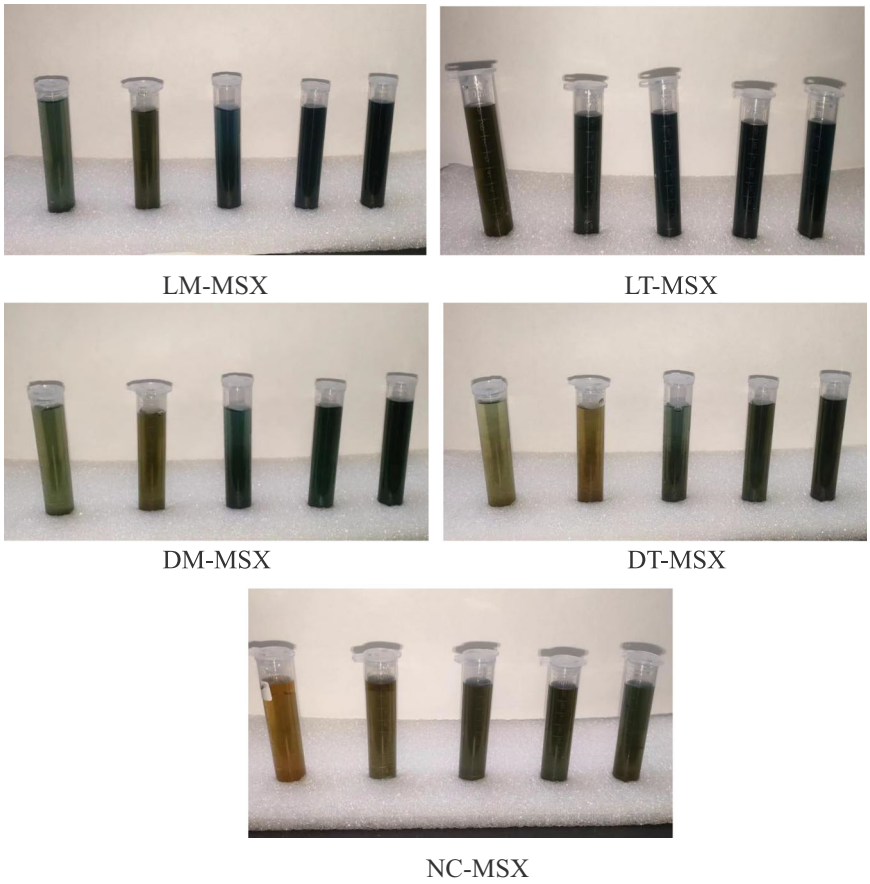

Fig. 6 Silica degradation image of NC-MSX, LT-MSX, DT-MSX, LM-MSX, and DM-MSX with the same carrier weight

was observed because a quite small amount of NMS was absorbed on the outer surface of the carrier, and this condition did not impact drug release because the small portion of NMS can be dissolved and released first.

3.2.3 FT-IR

Herein, NMS loaded L-BMSX was explained as an example for Fig. 9A. NMS presented its characteristic peaks, and typical peaks included the asymmetric stretching vibrations of nitro occurring between 1520 and 1590 cm^{-1}, symmetric stretching vibrations of nitro in the range of 1340–1380 cm^{-1}, and N–H stretching vibration (sulfonamide) around 3300 cm^{-1}. After loading into carriers, most drug peaks were covered, and the typical characteristic peaks of asymmetric stretching vibrations of nitro and symmetric stretching vibrations of nitro displayed a wavenumber shift. For example, the asymmetric stretching vibrations of nitro for NMS were displayed at 1589.6 cm^{-1}, while NMS loaded LT-MSX appeared at 1527.3 cm^{-1}, and the peak moved to the short wave direction, which can indicate that a hydrogen bond was formed between LT-MSX and NMS.

3.2.4 In vitro drug release

According to the results of drug release in Fig. 10, the release of drug-loaded carriers was higher than that of the raw drug because the two model drugs were crystalline drugs and the drug-loaded carriers were amorphous, and the conversion of drug form resulted in greater solubility and faster release than the raw drug [36–40]. It was obvious that the drug release of NMS loaded L-BMSX, NMS loaded M-BMSX, and NMS loaded H-BMSX was faster than NMS loaded BMSX, which demonstrated that the addition of HPMC in MSX assisted drug release, possibly because HPMC belonged to a water-soluble polymer. Also, the drug release of NMS loaded LT-MSX, NMS loaded DT-MSX, NMS loaded LM-MSX, and NMS loaded DM-MSX was faster than NMS loaded NC-MSX, which was also related to the reason that small molecules belonged to water-soluble molecules. Based on the above results, it was revealed that water-soluble molecules in MSX can be favorable for drug release Fig. 11.

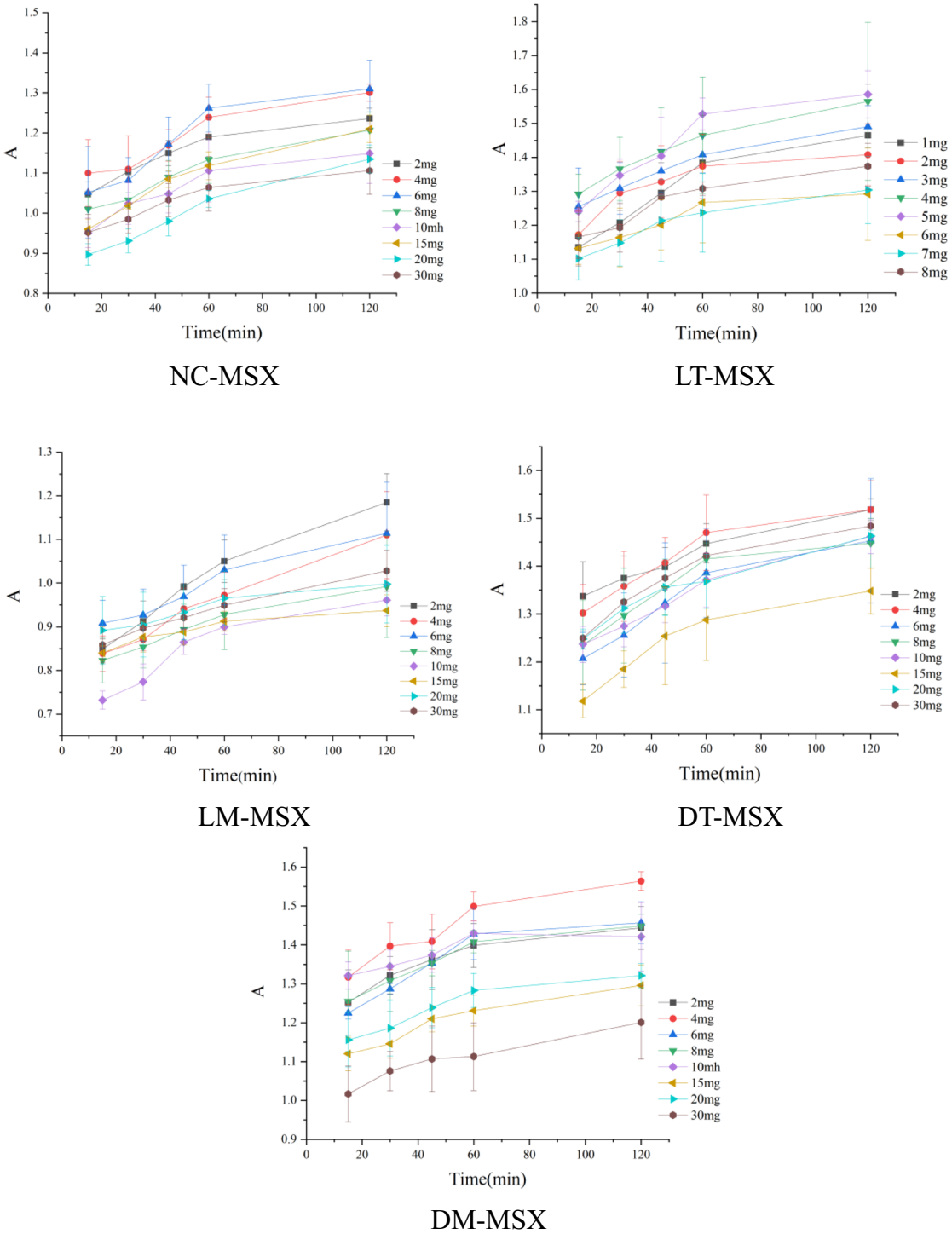

Fig. 7 Silica degradation of NC-MSX, LT-MSX, DT-MSX, LM-MSX, and DM-MSX

3.2.5 Anti-inflammatory experiment in rats

According to the anti-inflammatory results of rats, the drug-loaded carriers of the two model drugs had good anti-inflammatory effects, and the swelling degree of the rats' toes increased first and then gradually decreased, indicating that the inflammatory model was successfully induced [41]. When NMS was used as the model drug,

Table 2 Drug loading capacity of drug-loaded carriers

Sample	Drug loading capacity (%)
NMS loaded BMSX	20.70 ± 2.04
NMS loaded L-BMSX	18.55 ± 0.62
NMS loaded M-BMSX	19.21 ± 0.31
NMS loaded H-BMSX	23.72 ± 0.59
NMS loaded LT-MSX	21.26 ± 0.04
NMS loaded DT-MSX	24.66 ± 0.06
NMS loaded LM-MSX	11.30 ± 0.04
NMS loaded DM-MSX	12.41 ± 0.07
NMS loaded NC-MSX	24.33 ± 0.06

the swelling inhibition rate of NMS loaded L-BMSX was the highest. As shown in Table 3, the swelling inhibition rate of NMS loaded L-BMSX was 59.87% at 180 min, while that of NMS was 31.79%. The swelling inhibition rate of NMS loaded L-BMSX, NMS loaded M-BMSX, and NMS loaded H-BMSX were respectively 1.8 times, 1.3 times, and 1.6 times as much as NMS. The anti-inflammatory effect of NMS loaded L-BMSX was the best among the three groups. The above result highlighted that HPMC in MSX contributed to obtain a superior anti-inflammatory effect of NMS owing to its

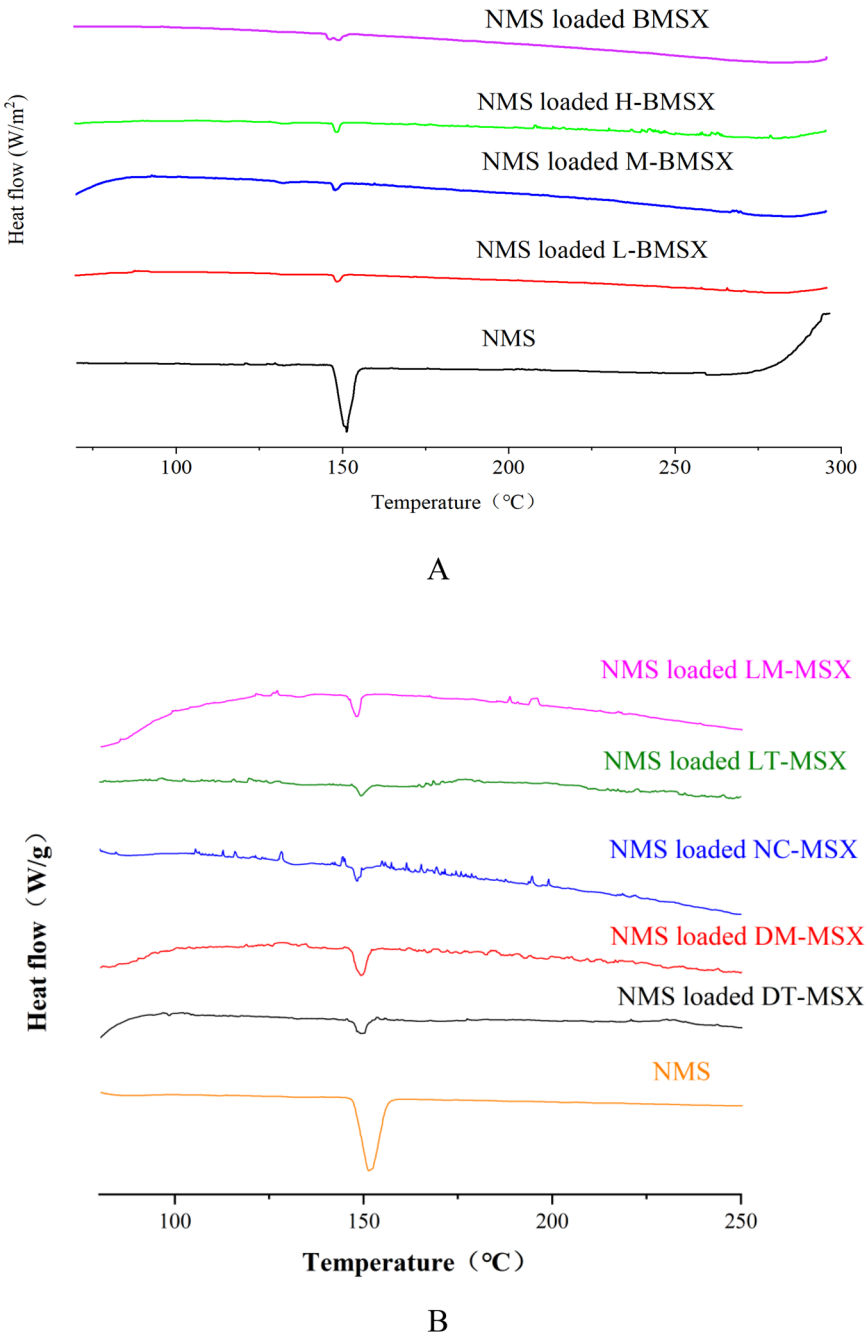

Fig. 8 DSC curves of NMS as well as NMS loaded carriers

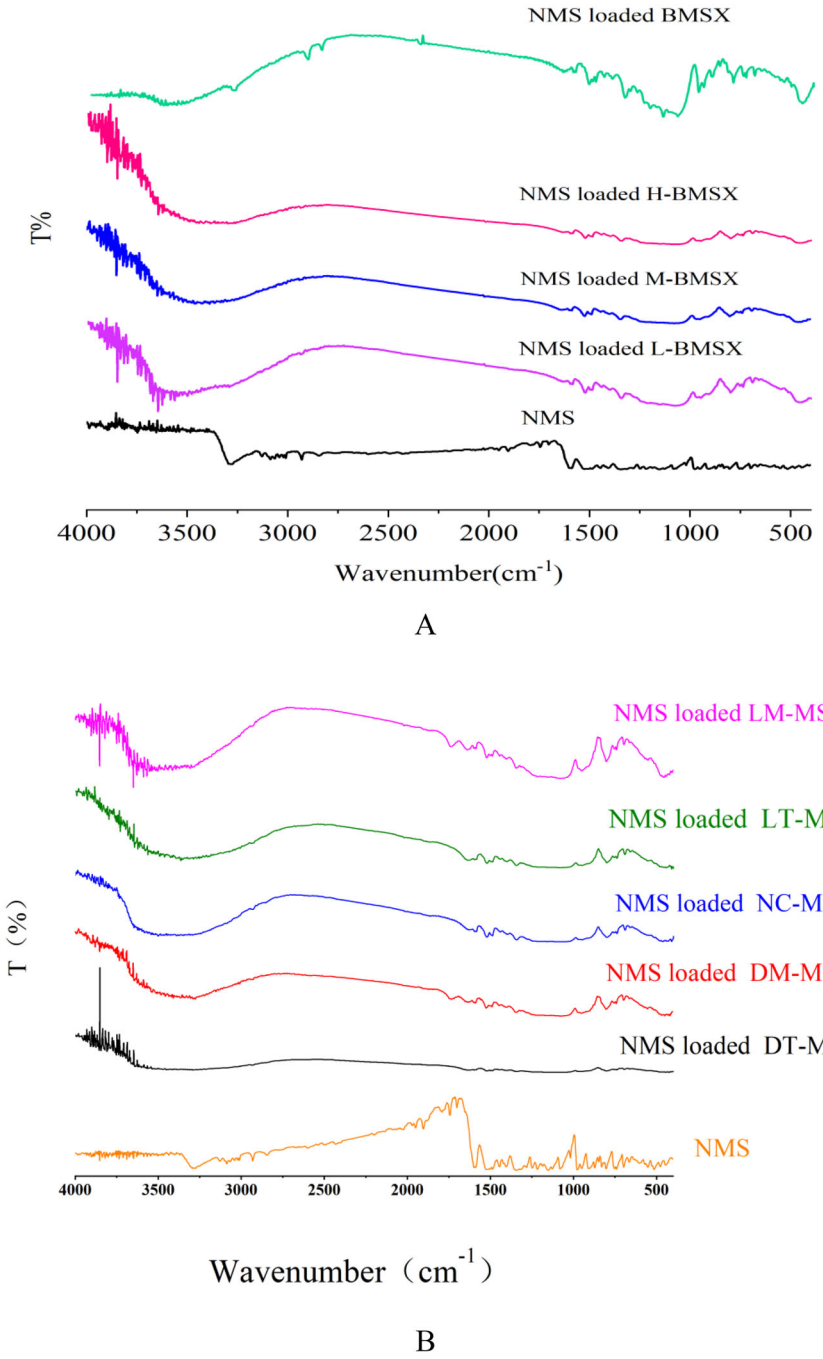

Fig. 9 IR spectra of NMS as well as NMS loaded carriers

faster drug release rate. It also reflected that faster drug release contributed by drug crystalline conversion and water-soluble polymer shouldered more important roles to achieve superior anti-inflammatory effect, though the silica degradation of NMS loaded L-BMSX, NMS loaded M-BMSX, and NMS loaded H-BMSX were a little slower than NMS loaded L-BMSX.

As for NMS loaded NC-MSX, NMS loaded LT-MSX, NMS loaded DT-MSX, NMS loaded LM-MSX, and NMS loaded DM-MSX, the swelling inhibition rate of NMS loaded LT-MSX and NMS loaded DT-MSX was better than that of NMS loaded NC-MSX because drug release and silica degradation of NMS loaded LT-MSX and NMS loaded DT-MSX were faster. However, NMS loaded LM-MSX and NMS loaded DM-MSX presented significantly weaker anti-inflammatory effect than NMS loaded NC-MSX, which was mainly because the silica degradation of NMS loaded LM-MSX and NMS loaded

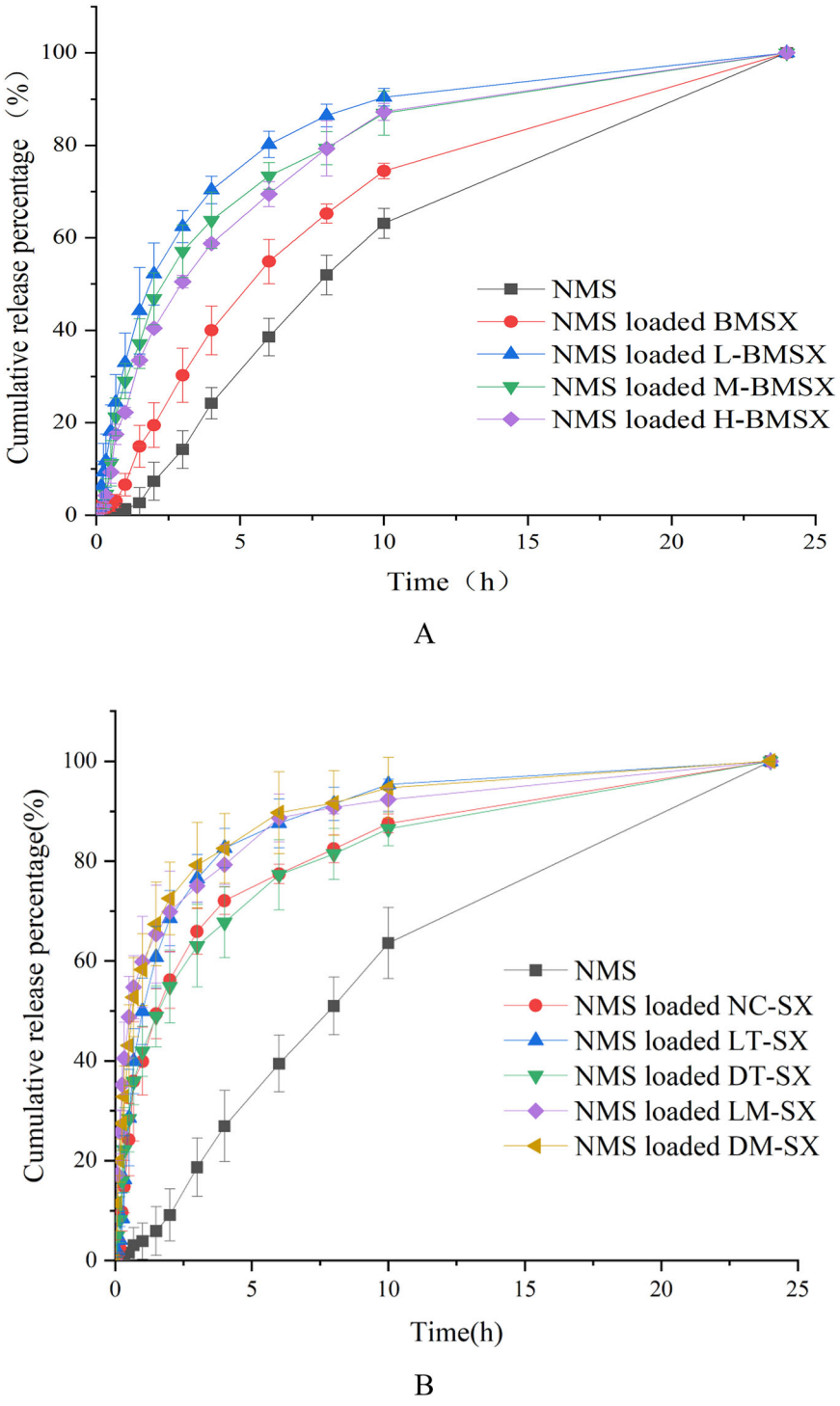

Fig. 10 In vitro release of NMS as well as NMS loaded carriers

DM-MSX was slower than NMS loaded NC-MSX, though their drug release was faster. NMS loaded LM-MSX presented the worst anti-inflammatory effect compared to NMS loaded DM-MSX owing to its slower silica degradation. It was clear that for water-soluble small molecules in MSX, silica degradation was the most important factor for anti-inflammatory effect, and faster silica degradation contributed to get better anti-inflammatory function. Among all these carriers, LT-MSX and DT-MSX turned out to be the best candidate for NMS owing to their fast drug release and silica degradation.

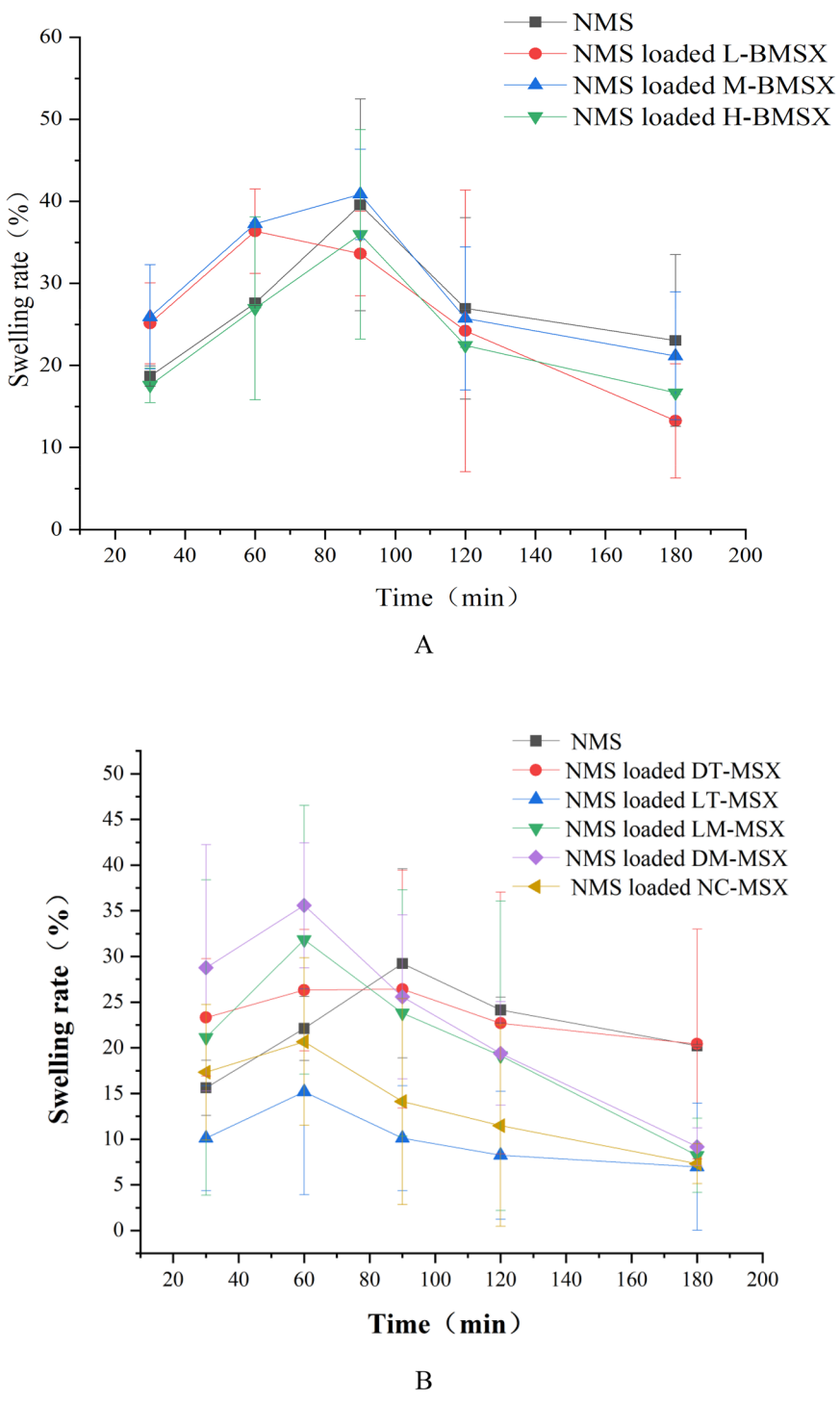

Fig. 11 Swelling inhibition rate of NMS as well as NMS loaded carriers

4 Conclusion

In the present study, MSX carriers either modified by small molecules or a polymer were synthesized using a biomimetic method and applied for loading poorly water-soluble NMS. All these carriers were composed of multiple silica particles with pores and similar morphology and structure, and no significant differences were observed. They presented good drug loading effects. Compared with the model drug, the melting point peak of the drug-loaded carrier was largely decreased, and the crystalline form was successfully converted to the amorphous form, leading to obtain faster drug release. HPMC in MSX contributed to obtain a superior anti-inflammatory effect of NMS owing to its faster drug release rate. The swelling inhibition rate of NMS loaded LT-MSX and NMS loaded DT-MSX was the

Table 3 Swelling inhibition rate of drug-loaded carriers

Sample	Swelling inhibition rate (%)
NMS loaded BMSX	31.79
NMS loaded L-BMSX	59.87
NMS loaded M-BMSX	40.43
NMS loaded H-BMSX	50.77
NMS loaded LT-MSX	77.85
NMS loaded DT-MSX	75.68
NMS loaded LM-MSX	27.22
NMS loaded DM-MSX	48.82
NMS loaded NC-MSX	70.38

best, owing to their fast drug release and silica degradation. All of the above can provide instruction for improving the solubility of poorly soluble drugs and enhancing the efficacy of anti-inflammatory drugs.

Data availability

Data can be provided as required.

Acknowledgements This study was supported by Liaoning Provincial Science and Technology Project Innovation Ability Improvement Joint Fund (2022-NLTS-14-06); National Natural Science Foundation of China (no. 82104114); Shenyang Young and middle-aged scientific and technological innovation talent support program from Shenyang Bureau of Science and Technology (no. RC220022); Shenyang Science and Technology Plan Project Social Governance Science and Technology Special Project (21-108-9-11); Team Construction Project of Liaoning Province Education Department (Grant No. LJ222410164002).

Author contributions Liu Yang: investigation. Nan Yan: formal analysis. Jing Li: original writing.

Compliance with ethical standards

Conflict of interest The authors declare no competing interests.

Ethics approval and consent to participate All animal experiments in this study were conducted according to the Guidelines for the Care and Use of Laboratory Animals that was authorized by the Ethics Review Committee for Animal Experimentation of Shenyang Medical College (Shenyang, Liaoning, China).

Publisher's note Springer Nature remains neutral with regard to jurisdictional claims in published maps and institutional affiliations.

References

1. Vallet-Regı´ M, Schuth F, Lozano D, Colilla M, Manzano M. Engineering mesoporous silica nanoparticles for drug delivery: Where are we after two decades?. Chem Soc Rev. 2022;51:13.
2. Sarkar S, Ekbal Kabir M, Kalita J, Manna P. Mesoporous silica nanoparticles: drug delivery vehicles for antidiabetic molecules. ChemBioChem. 2023;24:e202200672.
3. McCarthy CA, Ahern RJ, Dontireddy R, Ryan KB, Crean AM. Mesoporous silica formulation strategies for drug dissolution enhancement: a review. Expert Opin Drug Deliv. 2016;13:93–108.
4. Feng Y, Liao Z, Li M, Zhang H, Li T, Qin X, et al. Mesoporous silica nanoparticles-based nanoplatforms: basic construction, current state, and emerging applications in anticancer therapeutics. advanced healthcare. Materials. 2023;12:e2201884.
5. Liu J, Liu J, Wang Y, Chen F, He Y, Xie X, et al. Bioactive mesoporous silica materials-assisted cancer immunotherapy. Biomaterials. 2025;315:122919.
6. Wagner J, Gößl D, Ustyanovska N, Xiong M, Hauser D, Zhuzhgova O, et al. Mesoporous silica nanoparticles as pH-responsive carrier for the immune-activating drug resiquimod enhance the local immune response in mice. ACS Nano. 2021;15:4450–66.
7. Li J, Du X, Zheng N, Xu L, Xu J, Li S. Contribution of carboxyl modified chiral mesoporous silica nanoparticles in delivering doxorubicin hydrochloride in vitro: pH-response controlled release, enhanced drug cellular uptake and cytotoxicity. Colloids Surf B Biointerfaces. 2016;141:374–81.
8. Zhou Y, Liu K, Zhang H. Biomimetic mineralization: from microscopic to macroscopic materials and their biomedical applications. ACS Appl Bio Mater. 2023;6:3516–31.
9. Nie Z, Zhang Y, Tang R, Wang X. Biomimetic mineralization: an emerging organism engineering strategy for biomedical applications. J Inorg Biochem. 2022;232:111815.
10. Prince E. Designing biomimetic strain-stiffening into synthetic hydrogels. Biomacromolecules. 2024;25:6283–95.
11. Li X, Li D, Liu Z. Superiority of biomimetic micelle-entrapped nanoporous silica xerogel to deliver poorly water-soluble itraconazole. RSC Adv. 2022;12:28422–32.
12. Tengjisi HY, Yang G, Fu C, Liu Y, Zhao CX. Biomimetic core-shell silica nanoparticles using a dual-functional peptide. J Colloid Interface Sci. 2021;581:185–94.
13. Qiu Y, Lin Y, Zhang G. Unique silica biomimetic mineralization of acidic elastin-like polypeptides without hydroxyl and charged residues. Int J Biol Macromol. 2020;153:224–31.
14. Jiang Q, Wu L, Zheng Y, Xia X, Zhang P, Lu T, et al. Biomimetic micellar mesoporous silica xerogel performs superior nitrendipine dissolution, systemic stability and cellular transmembrane transport. Mater Sci Eng C Mater Biol Appl. 2021;118:111372.
15. Patwardhan SV. Biomimetic and bioinspired silica: recent developments and applications. Chem Commun. 2011;47:7567–82.
16. Panigrahy D, Gilligan MM, Serhan CN, Kashfi K. Resolution of inflammation: An organizing principle in biology and medicine. Pharmacol Ther. 2021;227:107879.

17. Massironi S, Viganò C, Palermo A, Pirola L, Mulinacci G, Allocca M, et al. Inflammation and malnutrition in inflammatory bowel disease. Lancet Gastroenterol Hepatol. 2023;8:579–90.
18. Sahoo DK, Heilmann RM, Paital B, Patel A, Yadav VK, Wong D, et al. Oxidative stress, hormones, and effects of natural antioxidants on intestinal inflammation in inflammatory bowel disease. Front Endocrinol. 2023;14:1217165.
19. Illig D, Kotlarz D. Dysregulated inflammasome activity in intestinal inflammation-Insights from patients with very early onset IBD. Front Immunol. 2022;13:1027289.
20. Li HM, Gou R, Liao JY, Wang Y, Qu R, Tang Q, et al. Recent advances in nano-targeting drug delivery systems for rheumatoid arthritis treatment. Acta Mater Med. 2023;2:23–41.
21. Sanchez-Lopez E, Coras R, Torres A, Lane NE, Guma M. Synovial inflammation in osteoarthritis progression. Nat Rev Rheumatol. 2022;18:258–75.
22. Kang S, Kim J, Park A, Koh M, Shin W, Park G, et al. TRIM40 is a pathogenic driver of inflammatory bowel disease subverting intestinal barrier integrity. Nat Commun. 2023;14:700.
23. Vunnam N, Young MC, Liao EE, Lo CH, Huber E, Been M, et al. Nimesulide, a COX-2 inhibitor, sensitizes pancreatic cancer cells to TRAIL-induced apoptosis by promoting DR5 clustering. Cancer Biol Ther. 2023;24:2176692.
24. Candelario-Jalil E. Nimesulide as a promising neuroprotectant in brain ischemia: new experimental evidences. Pharmacol Res. 2008;57:266–73.
25. Wang M, Liu S, Jia L, Zhang J, Du S, Gong J. Exploring the physical stability of three nimesulide-indomethacin co-amorphous systems from the perspective of molecular aggregates. Eur J Pharm Sci. 2020;147:105294.
26. Gou K, Wang Y, Guo X, Wang Y, Bian Y, Zhao H, et al. Carboxyl-functionalized mesoporous silica nanoparticles for the controlled delivery of poorly water-soluble non-steroidal anti-inflammatory drugs. Acta Biomater. 2021;134:576–92.
27. Wang WH, Liang HT, Yang-Wang YT, Shih CJ. Synthesis of hierarchically mesoporous silica with encapsulated avobenzone as a UV protection filter. RSC Adv. 2020;10:15846–52.
28. Morishige K. Pore size distribution analysis using developing hysteresis of nitrogen in the cylindrical pores of silica. Langmuir. 2022;38:4222–33.
29. Gao JM, Yan Z, Ma S, Guo Y. Novel process for high value utilization of high-alumina fly ash: valuable metals recovery and mesoporous silica in situ preparation. RSC Adv. 2024;14:1782–93.
30. Shakeri M, Khatami Shal Z, Van Der Voort P. An overview of the challenges and progress of synthesis, characterization and applications of plugged SBA-15 materials for heterogeneous catalysis. Materials. 2021;14:5082.
31. Zhang H, Li M, Li J, Agrawal A, Hui HW, Liu D. Superiority of mesoporous silica-based amorphous formulations over spray-dried solid dispersions. Pharmaceutics. 2022;14:428.
32. Tu B, Jonnalagadda S. Amorphous stabilization of BCS II drugs using mesoporous silica. Int J Pharm. 2024;663:124555.
33. Baumgartner A, Planinšek O. Application of commercially available mesoporous silica for drug dissolution enhancement in oral drug delivery. Eur J Pharm Sci. 2021;167:106015.
34. Elmowafy M, Alruwaili NK, Ahmad N, Kassem AM, Ibrahim MF. Quercetin-Loaded mesoporous silica nanoparticle-based lyophilized tablets for enhanced physicochemical features and dissolution rate: formulation, optimization, and in vitro evaluation. AAPS PharmSciTech. 2022;24:6.
35. Guo Y, Wang H, Zhu Q, Mao Y, Wen X, Zhang X, et al. Exploration of enalapril-lacidipine co-amorphous system with superior dissolution, in vivo absorption and physical stability via incorporated into mesoporous silica. Eur J Pharm Sci. 2025;207:107033.
36. Ji H, Shi X. Hydroxypropyl methylcellulose E5 with molecular energy-enhancement ability contributes to improving wettability, drug delivery and taste masking effect for curcumin solid dispersions. Int J Biol Macromol. 2025;303:140715.
37. Maleki A, Kettiger H, Schoubben A, Rosenholm JM, Ambrogi V, Hamidi M. Mesoporous silica materials: From physico-chemical properties to enhanced dissolution of poorly water-soluble drugs. J Control Release. 2017;28:329–47.
38. Ibrahim AH, Smått JH, Govardhanam NP, Ibrahim HM, Ismael HR, Afouna MI, et al. Formulation and optimization of drug-loaded mesoporous silica nanoparticle-based tablets to improve the dissolution rate of the poorly water-soluble drug silymarin. Eur J Pharm Sci. 2020;142:105103.
39. Wang X, Li C, Fan N, Li J, Zhang H, Shang L, et al. Amino functionalized chiral mesoporous silica nanoparticles for improved loading and release of poorly water-soluble drug. Asian J Pharm Sci. 2019;14:405–12.
40. Xin W, Wang L, Lin J, Wang Y, Pan Q, Han Y, et al. Mesoporous silica nanoparticles with chiral pattern topological structure function as “antiskid tires” on the intestinal mucosa to facilitate oral drugs delivery. Asian J Pharm Sci. 2023;18:100795.
41. Hsieh CY, Wang CC, Tayo LL, Deng SX, Tsai PW, Lee CJ. In vitro and in vivo anti-osteoarthritis effects of tradition Chinese prescription Ji-Ming-San. J Ethnopharmacol. 2023;305:116084.